

Supplemental materials

The dynamics of individual nucleosomes controls the chromatin condensation pathway: direct AFM visualization of variant chromatin.

Fabien Montel, Hervé Menoni, Martin Castelnovo, Jan Bednar, Stefan Dimitrov, Dimitar Angelov and Cendrine Faivre-Moskalenko

1 - Biochemical analysis of conventional and variant mono-nucleosomes

We provide here a schematic of the amino acid sequence for 3 different proteins used for nucleosome reconstitution: H2A, H2A.Bbd and Bdh.H2A. It indicates where the docking domain of H2A.Bbd (in green) is replaced by that of H2A (in blue) in Bbd.ddH2A, and also highlight (in red) the position of the amino acids contributing to the acidic patch (1-3).

H2A.1 human	M---SGRGKQGGKARAKAKTRSSRAGLQFPVGRVHRLLRKGNYSERVGAGAPVYLAAVLEYLTAEILELA
H2A.Bbd human	MPRRRRRRGSSGAGGRGRTCSRTVRAELSFVSQVERSLREGHYAQLSRTAPVYLAAVIEYLTAKVLELA
Bbd.ddH2A	MPRRRRRRGSSGAGGRGRTCSRTVRAELSFVSQVERSLREGHYAQLSRTAPVYLAAVIEYLTAKVLELA
H2A.1 human	GNAARDNKKTRII PRHLQLAIRNDEELNKKLLGRVTIAQGGVLPNIQAVLLPKKTESHKAKGK
H2A.Bbd human	GNEAQNSGERNITPLLLDMVHNDRLSTLFTTTISQ--VAPGED
Bbd.ddH2A	GNEAQNSGERNITPRHLQLAIRNDEELNKKLLGRVTIAQGGVLPNIQAVLLPKKTESHKAKGK

docking domain

Figure S1: Sequence alignment of the human H2A (in blue), the human H2A.Bbd (in green) and the chimeric histone Bbd.ddH2A (in blue and green). The docking domain is indicated by a dashed line. The amino acid contributing to the acidic patch in the H2A nucleosome are highlighted in red, and in purple are the corresponding amino acids in the variant H2A.Bbd or chimeric Bbd.ddH2A histones that do not contribute anymore to this acidic patch.

Then we present the result of Micrococcal nuclease digestion experiments on conventional H2A, variant H2A.Bbd and chimeric Bbd.ddH2A mono-nucleosomes (Figure S2). The accessibility of mono-nucleosomes of each type was probed by Micrococcal Nuclease (Mnase) digestion method (Fig. S1b): conventional H2A (lanes 1 to 4), variant H2A.Bbd (lanes 6 to 10) and chimeric variant Bbd.ddH2A (lanes 11 to 14). As previously observed, the H2A.Bbd mono-nucleosome is more accessible than the conventional one, as the 147 bp band, corresponding to the conventional Nucleosomal Core Particle (NCP), remains visible for only very little time (~1 min) for H2A.Bbd, whereas it is still visible on the conventional mono-nucleosome at the end of the experiment (12 minutes). The change in the digestion pattern is interpreted as a more relaxed structure for the H2A.Bbd nucleosome. In the case of Bbd.ddH2A, the overall digestion pattern for this chimeric variant mono-nucleosome is intermediate between the conventional and the H2A.Bbd variant nucleosomes.

The 147 bp band remains visible a little longer (at least 2.5 min) but the accessibility is again clearly stronger than for the conventional H2A nucleosome. The results of our AFM

study on mono-nucleosomes, which found a high dynamics of DNA opening for Bbd.ddH2A nucleosome, are compatible with these micrococcal nuclease digestion patterns. Therefore, despite the longer length of DNA wrapped on average around the Bbd.ddH2A octamer, the enzyme accessibility will be higher than the conventional H2A nucleosome, thereby resulting in a pattern close to the H2A.Bbd nucleosome

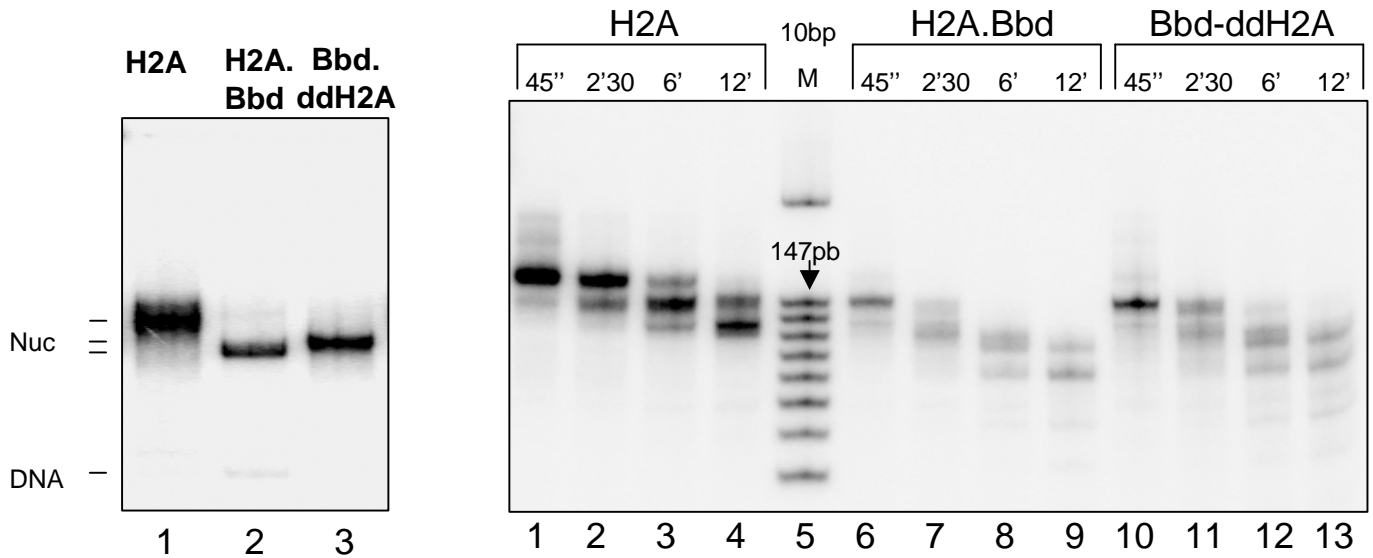


Figure S2: Biochemical characterization of conventional H2A, variant H2A.Bbd and chimeric Bbd.ddH2A mono-nucleosomes. (a) EMSA analysis of the reconstituted nucleosomes. The position of the nucleosomes (nuc.) and the naked DNA are indicated on the left part of the figure. (b) Micrococcal nuclease digestion kinetics of nucleosomes. Identical amount of nucleosome were digested (in presence of 100 µg/ml plasmid DNA) with 8U/ml of micrococcal nuclease for the indicated times. The reaction was stopped by addition of 20 mM EDTA and 0,1 mg/ml proteinase K, 0,1% SDS. DNA was isolated and run on a 10% polyacrilamide gel. The lane M shows the scan of the gel 10 bp marker DNA.

Supplemental methods: The 255 DNA fragment, containing the 601 nucleosome positioning sequence in the middle was obtained by polymerase chain reaction (PCR) amplification from plasmid pGem-3Z-601 (kindly provided by B Bartholomew and J Widom). Labeling was performed by adding 30 µCi of [α - 32 P]CTP to the PCR reaction. For nucleosome reconstitution, carrier DNA (150–200 bp, 2 µg) and 50 ng of 32 P labeled DNA were mixed with equimolar amount of histone octamer in nucleosome reconstitution buffer NRB (2 M NaCl, 10 mM Tris pH 7.4, 1 mM EDTA, 5 mM β -mercaptoethanol), and reconstitution was performed by the salt dialysis procedure (4).

2 – ECM validation of compact conformation for conventional chromatin

We provide in this section electron cryo-microscopy pictures of nucleosomal arrays reconstituted on the same 15 repeat of 601 DNA sequence as used in the AFM experiments. Furthermore, the buffer conditions are essentially similar to the ones for AFM imaging. The images clearly support the compact conformation visualized by AFM. Since cryoEM experiments are performed in solution (no adsorption or drying is required), the chromatin

fiber is in a real 3D configuration. The observed pictures strongly support the relevance of our AFM quantitative study.

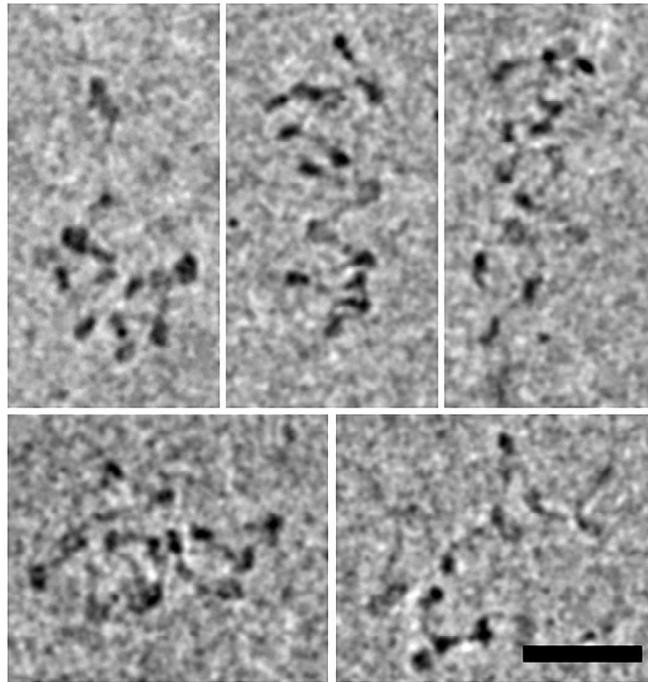


Figure S3: A representative configurations of nucleosomal arrays (15 nucleosomes) in 10 mM Tris and 5 mM NaCl in absence of the linker histone. Scale bar = 50 nm.

Supplemental methods: The samples for electron cryo-microscopy were prepared as described earlier (3). Shortly, 3 μ l of the sample solution at concentration of 200 μ g/ml of DNA was applied to an electron microscopy grid covered with perforated supporting film. Most of the sample was removed by blotting (Whatmann No 1 filter paper) for approximately one second, and the grid was immediately plunged into liquid ethane held at -183°C . The sample was then transferred without rewarming into Tecnai Sphera G²⁰ electron microscope using Gatan 626 cryo-specimen holder. The images were recorded at 80 kV accelerating voltage and direct microscope magnification 14 500 \times using Gatan UltraScanTM 1000 slow scan CCD camera (giving final pixel size 0.7 nm) with underfocus of 2.7 μ m. The low dose operating mode was used with the total electron dose not exceeding 15 electrons per square \AA . The ionic conditions were identical to those used for AFM experiments (Tris 10mM pH = 7.4, EDTA 1mM, NaCl 5 mM).

3- Numerical simulations

The relevant exact geometrical relationships are summarized on figure S2: one links the distance between nucleosome centers with the DNA linker length, the angle associated to the entry/exit points of DNA on the NCP with the angle between consecutive lines joining nucleosome centers (the latter angle is more convenient for the simulations), and finally the DNA linker length with the opening angle θ . $L_0 = 50 * 0.34$ nm is the linker length of our construction. The radius $R = 4.5$ nm is the distance from the center of nucleosome to the main path of DNA. The angle $\theta_0 = \pi/2$ is chosen such that 147 bp wrap 1.75 turns around the nucleosome.

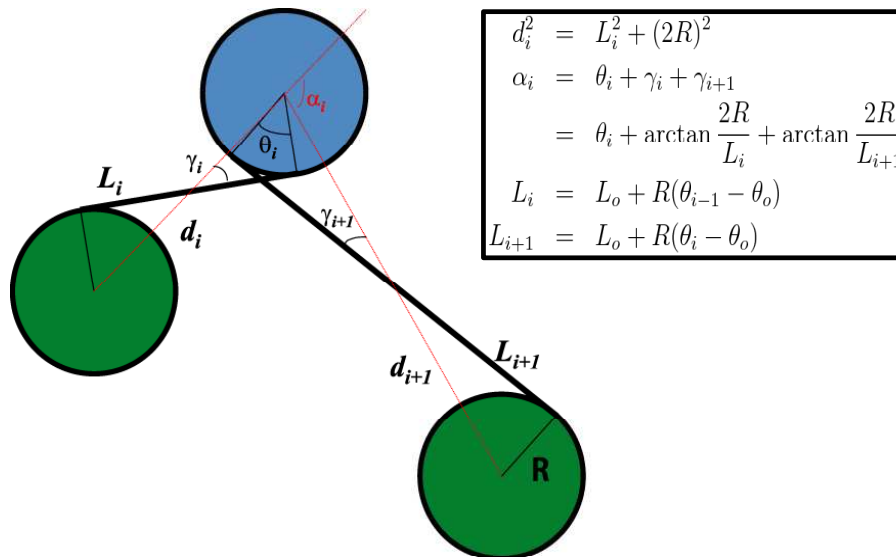


Figure S4 : Basic drawing of the geometrical model used for the simulation of nucleosomal arrays showing the relation between the DNA complexed length, the linker length and the nucleosome opening angle.

Representative snapshots of simulated fibers and the corresponding Kratky plots of the structure factors are shown in Figure S5.

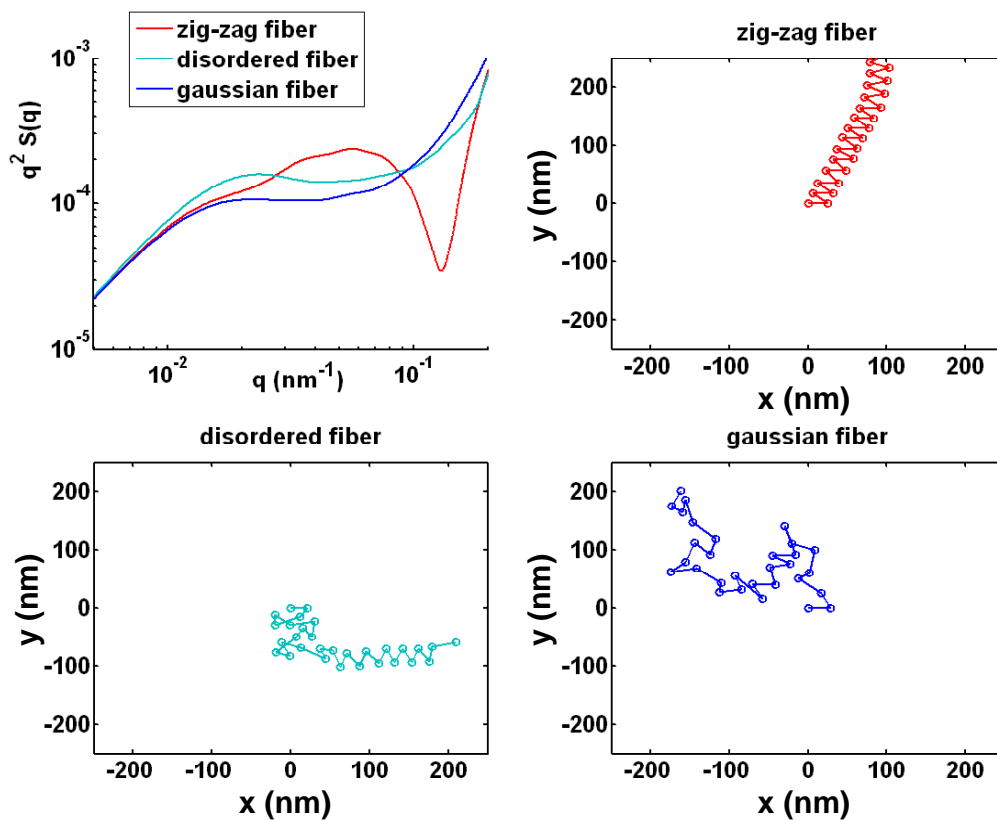


Figure S5 : Simulation of ‘model’ fibers of 30 nucleosomes. Kratky plot $q^2 S(q)$ vs q for a zigzag fiber (red), a disordered fiber (light blue) and a gaussian fiber (blue). The structure factor is averaged over 500 realizations, and one typical realization is shown as an example.

4- Accuracy of both experimental and simulated Kratky plots

In this section we show the reliability of our Kratky plot analysis by comparing on the same figure the Kratky plots obtained for conventional and variant 30 repeat chromatin arrays including error bars (plotted as standard error on the mean value of $(q^2S(q)/N)$) together with the corresponding simulated chains. Note that for the simulations, more than 100 runs is enough to ensure negligible standard error (compared to experimental curves).

We observe clearly that from a statistical point of view, the ‘compaction’ peak is significant, even for the lowest statistics of our set of measurements (~ 20 to 50 chains for the 32 repeat nucleosomal arrays). In other words, this confirms the existence of clearly separated typical behaviors: a ‘gaussian plateau’ and a pronounced peak regimes corresponding respectively to a gaussian variant chromatin chain and a compacted conventional chromatin fiber.

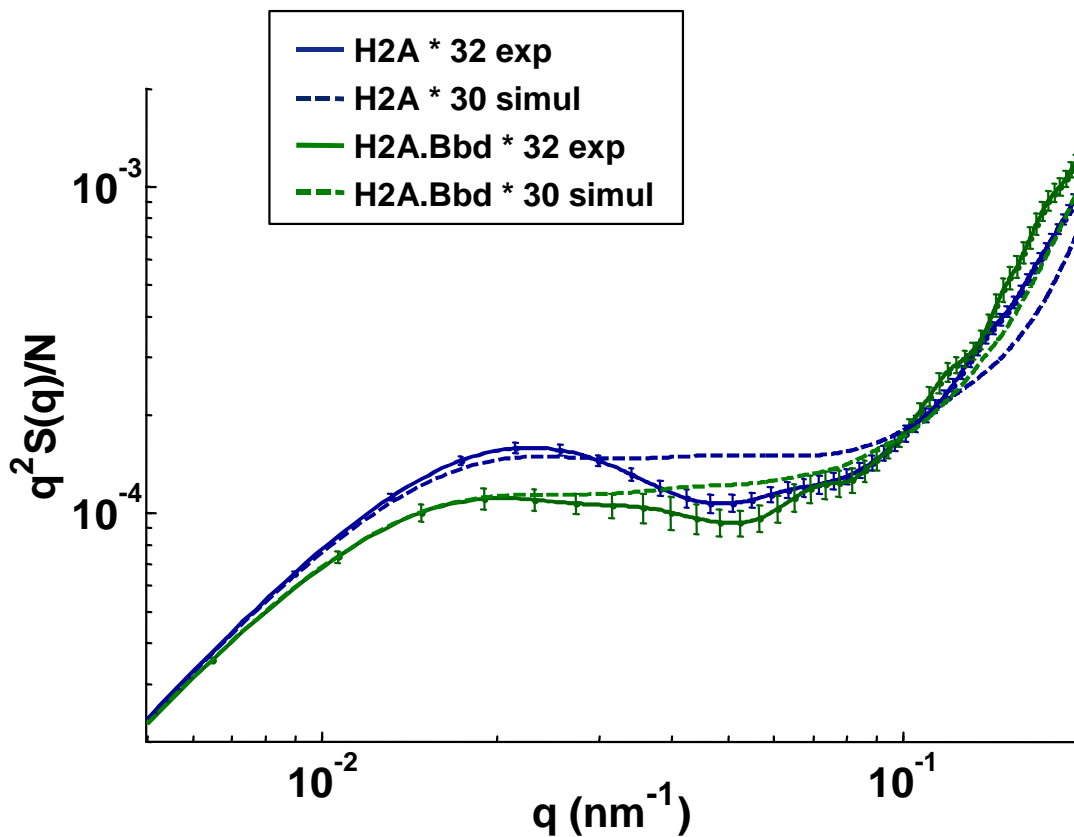


Figure S6: Experimental Kratky plots (solid lines) for nucleosomal arrays reconstituted on 32 repeat 601 DNA fragments with (dark blue) H2A conventional histone and (dark green) H2A.Bbd variant histones. The errorbar corresponds to the standard error from the mean value of $(q^2S(q)/N)$ at each wave vector q (error = σ/\sqrt{N} where σ is the standard deviation on the mean and N the number of events in the distribution), for the sake of clarity of the figure, only 1 out of 10 is plotted. Corresponding Kratky plots of structure factors averaged over 500 simulated 30 repeat nucleosomal arrays (dotted lines) is calculated with the parameters of (dark blue) the conventional H2A mono-nucleosome (average angle $\theta = 0.5 \pi$ and flexibility $\sigma_\theta = 0.4 \pi$) and (dark green) the variant H2A.Bbd mono-nucleosome ($\theta = 0.7 \pi$ and $\sigma_\theta = 0.7 \pi$).

5- Experimental and simulated Kratky plots for Bbd.ddH2A chromatin

In order to decipher the role of each parameter (opening angle θ and flexibility σ_θ), we performed simulation with several combinations of the experimental values found for these two parameters. The low angle and low flexibility couple value (0.5π , 0.4π) corresponds to conventional H2A nucleosomes, whereas large angle and large flexibility couple (0.7π , 0.7π) describes the variant H2A.Bbd nucleosomal array. Interestingly when the opening angle is low but the flexibility remains large (0.5π , 0.7π) which corresponds to the chimeric Bbd.ddH2A nucleosomal array), the simulated Kratky plot is very close to the one of the simulated variant chromatin.

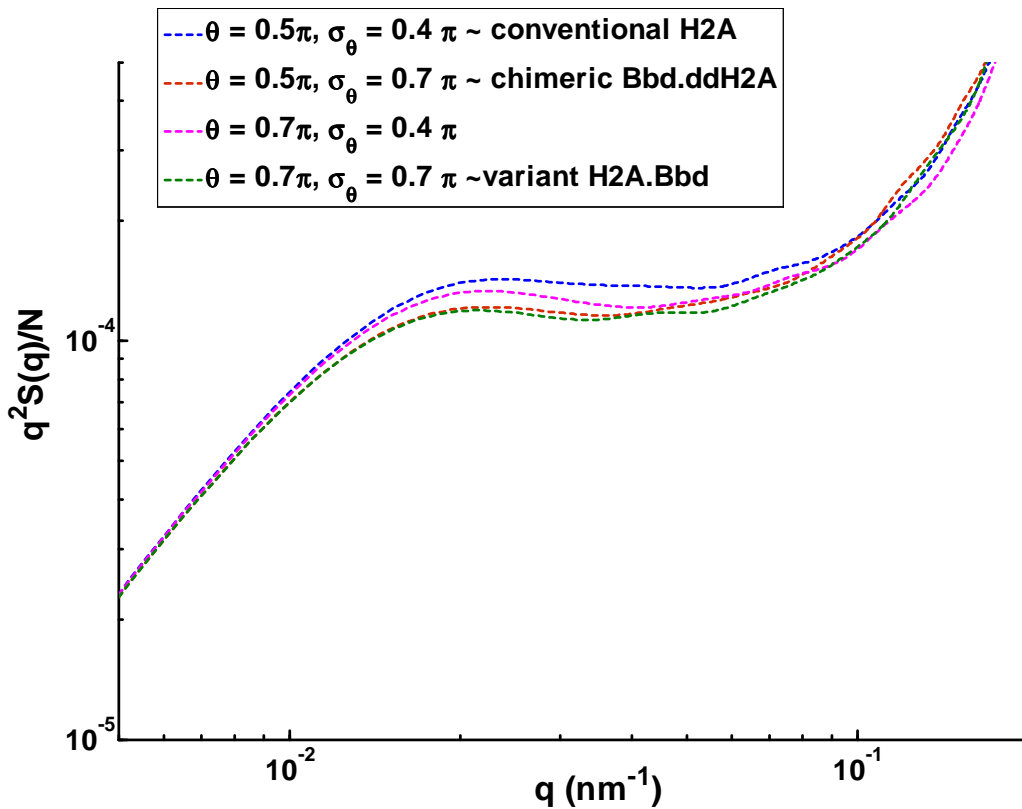


Figure S7 : Kratky plot $q^2 S(q)$ vs q for simulated nucleosomal arrays of 30 nucleosomes, for various combinations of the two parameters : θ , the opening angle and σ_θ the fluctuation amplitude for this θ angle. According to the measurements performed on the mono-nucleosomes (3), we chose ($\theta=0.5\pi$; $\sigma_\theta = 0.5\pi$) for conventional chromatin, ($\theta=0.7\pi$; $\sigma_\theta = 0.7\pi$) for H2A.Bbd variant nucleosomal array and ($\theta=0.5\pi$; $\sigma_\theta = 0.7\pi$) for chimeric Bbd.ddH2A chromatin. The structure factor is averaged over 200 realizations. Only geometrical model and excluded volume effects are taken into account.

This is consistent with what is observed experimentally and demonstrates that the flexibility parameter is the main ingredient to chromatin compaction. This is further shown by the last condition (large opening angle but low flexibility (0.7π , 0.4π)) that exhibits a Kratky plot similar to the simulated conventional chromatin Kratky plot.

6- References

1. Zhou, J., J. Y. Fan, D. Rangasamy, and D. J. Tremethick. 2007. The nucleosome surface regulates chromatin compaction and couples it with transcriptional repression. *Nat Struct Mol Biol* 14:1070-1076.
2. Bao, Y., K. Konesky, Y. J. Park, S. Rosu, P. N. Dyer, D. Rangasamy, D. J. Tremethick, P. J. Laybourn, and K. Luger. 2004. Nucleosomes containing the histone variant H2A.Bbd organize only 118 base pairs of DNA. *Embo J* 23:3314-3324.
3. Doyen, C. M., F. Montel, T. Gautier, H. Menoni, C. Claudet, M. Delacour-Larose, D. Angelov, A. Hamiche, J. Bednar, C. Faivre-Moskalenko, P. Bouvet, and S. Dimitrov. 2006. Dissection of the unusual structural and functional properties of the variant H2A.Bbd nucleosome. *Embo J* 25:4234-4244.
4. Mutskov, V., D. Gerber, D. Angelov, J. Ausio, J. Workman, and S. Dimitrov. 1998. Persistent interactions of core histone tails with nucleosomal DNA following acetylation and transcription factor binding. *Mol Cell Biol* 18:6293-6304.